JOURNAL OF MATERIALS SCIENCE 31 (1996) 232–241

Damage characterization of two-dimensional woven and three-dimensional braided SiC–SiC composites

P. PLUVINAGE, A. PARVIZI-MAJIDI, T. W. CHOU
Center for Composite Materials and Department of Mechanical Engineering, University of Delaware, Newark, DE 19716, USA

A comprehensive investigation of the room temperature behaviour of two-dimensional woven and three-dimensional braided SiC–SiC composites fabricated by the chemical vapour infiltration route has been conducted. A morphological study of the residual porosity in the composites revealed the existence of primarily two populations of pores: small intrayarn pores and larger interyarn pores. The sizes and the shapes of the two types of pores depended largely on the fibre architecture; the two step braided composite in which the majority of the fibre yarns were orientated along the axial direction exhibited the smallest pore size. The pore size and shapes in turn influenced the onset of damage in the composites under tensile loading. Damage was found to be initially matrix dominated, thus being essentially independent of the fibre architecture. At higher stress levels, however, fibre dominated damage prevailed. Unlike the tensile behaviour, where damage led to non-linearity in the stress–strain curve, the compressive behaviour of the composites was linear elastic almost up to failure. The off-axis tensile properties as well as compression after tension behaviour of the two-dimensional woven composites were also investigated. The information obtained from these tests provides the basis for the modelling of damage in these materials.

1. Introduction

SiC fibre reinforced SiC (SiC–SiC) composites fabricated by the chemical vapour infiltration (CVI) process have received considerable attention for high temperature structural applications [1–4]. The CVI route offers certain advantages for processing of ceramic matrix composites (CMCs). The low temperature of the process (900–1100 °C) minimizes fibre damage, and since densification is conducted under essentially no external pressure, fibre arrangement is undisturbed during the process. The technique is, therefore, particularly suitable for the infiltration of multidirectional fabric preforms where the preservation of an intricate fibre architecture during processing is desirable.

A relatively large volume of studies has been conducted on two-dimensional woven SiC–SiC composites [5]. Recently, attention has been directed towards three-dimensional woven or braided composite structures in order to meet mechanical and thermal property requirements along the thickness direction of composites used in gas turbines or heat exchangers. While extensive modelling and experimental data exist for three-dimensional textile polymer matrix composites [6], such knowledge is still very scarce for CMCs.

Among the existing three-dimensional textile preforms, the two step braids and four step braids are of particular interest. Both preforms provide through-the-thickness reinforcement, while the efficiencies in axial reinforcement are quite different. The yarn carrier arrangements in the braiding bed and their movements for two step and four step braidings are shown in Fig. 1a and b, respectively [6]. The two step braiding process is so named because it involves two distinct motions of each yarn carrier. The braid consists of an array of axial yarns arranged in a prescribed configuration, and braider yarns positioned on the perimeter of the axial array. The braider yarns, which move along alternating diagonals of the axial array, interlink the axials and hold them in the desired shape. The four step braiding process involved four distinct Cartesian motions of groups of yarn termed rows and columns. For a given step, alternating rows (columns) are shifted a prescribed distance relative to each other. The next step involves the alternate shifting of the columns (rows) a prescribed distance. The third and fourth steps involve simply the reverse shifting sequence of the first and second steps, respectively. A complete set of four steps is called a machine cycle.

The damage behaviour in unidirectional and cross-ply glass–ceramic matrix composites is highly anisotropic as shown in [7–9]. The behaviour of two-dimensional woven ceramic matrix composites processed by the CVI technique is further complicated by

0022–2461

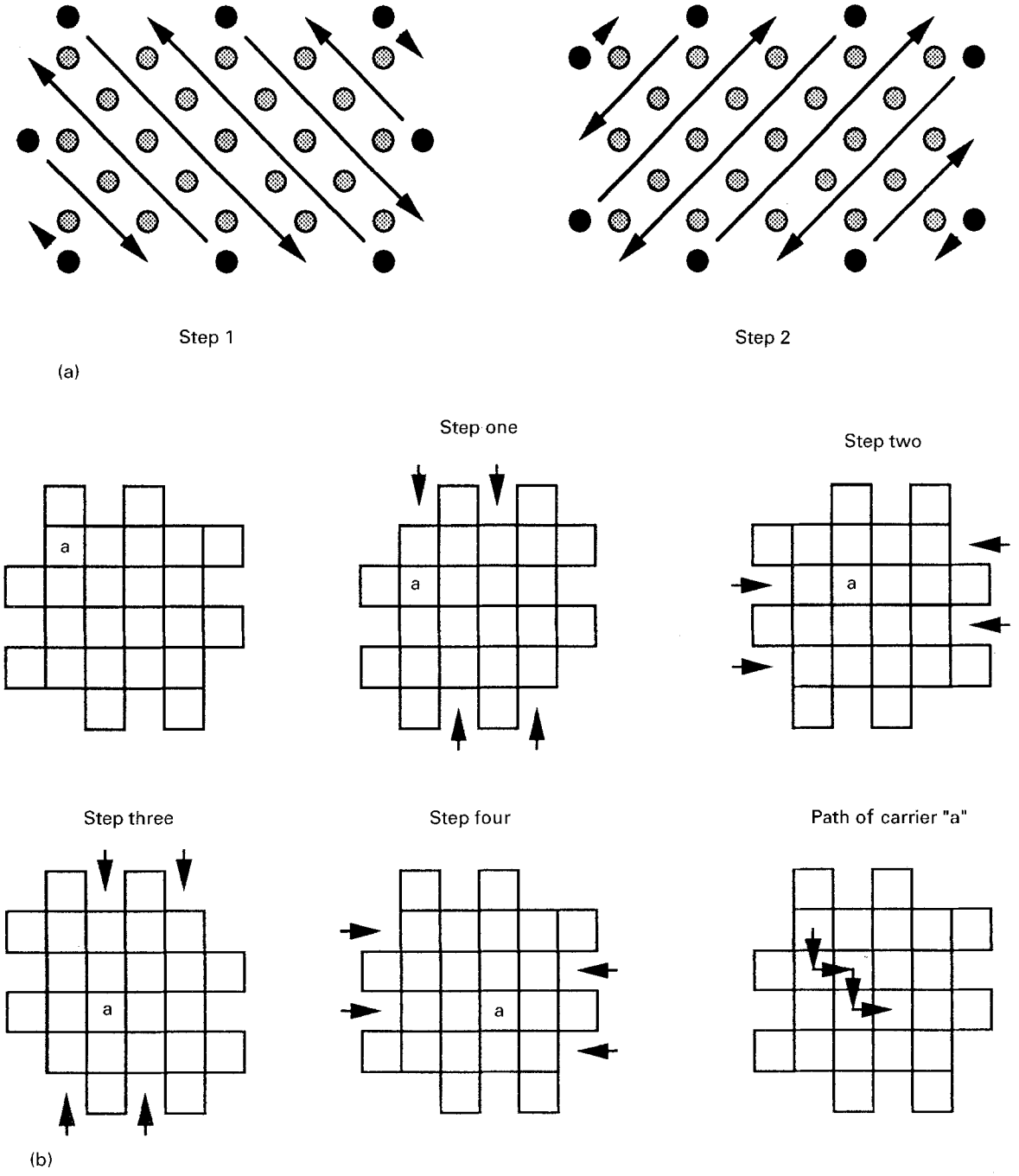

Figure 1 The yarn carrier arrangements and their movement for (a) the two step, and (b) the four step braiding process: (◎) axial yarn, (●) braider yarn.

the presence of fabrication induced pores which act as sites of stress concentrations [10, 11]. Major damage mechanisms, including matrix cracking, fibre–matrix debonding and fibre breakage, have been identified for glass–ceramic and ceramic matrix composites.

This paper examines the room temperature behaviour under tensile, compressive and flexural loading of two- and three-dimensional fabric SiC–SiC composites produced by CVI. The objective is to develop an understanding of the effects of fibre architecture on residual porosity, mechanical properties and composite damage behaviour. The data generated are to expand the experimental knowledge base for design with these materials, as well as to be used as input for modelling of damage and life prediction of SiC–SiC fabric composites.

2. Experimental procedure

2.1. Fibre architecture

Three different preforms, made of SiC (Nicalon) fibres were selected for this study: a two-dimensional plain weave fabric and two three-dimensional braided preforms. The two-dimensional plain weave fabric composite contains 40–45% fibre and 10–12% residual porosity, in volume. Each yarn contains 500 fibres and the fabric is balanced in the warp and weft directions.

The two three-dimensional preforms were fabricated at the Center for Composite Materials of University of Delaware. These included a two step braided preform and a four step braided preform. The two step braided preforms had about 80% of the yarns in the axial direction and the remaining 20% as braider yarns, thus giving rise to a structure that was highly

unidirectional. The axial and braider yarns each contained 2000 and 1000 fibres, respectively. The composite made with this preform had a fibre content of about 40% by volume and residual porosity ranging from 8 to 10%. In the four step braided preforms, all the yarns, each containing 2000 fibres, acted as braider yarns and were orientated at about $\pm 25°$ to the axial direction. The fibre volume content was about 40% and the residual porosity between 12 and 15%.

The SiC matrix infiltration of the two- and three-dimensional fabric preforms was conducted at E. I. DuPont de Nemours & Co. using a CVI technique. The infiltration conditions were identical for all three types of preforms.

2.2. Morphological study

Ceramic matrix composites densified by the CVI process exhibit residual pores. The pore morphology plays a significant role in the mechanical behaviour of composites. A morphological study, performed using image analysis [12], allowed the generation of statistical information about surface area, count, position, geometry and orientation of voids in the three materials.

The shape of the pores is dominated by the fibre architecture at the intrayarn and interyarn levels. Within each yarn, the progressive coating of the fibres creates longitudinal pores extending along the fibres. The cross-sections of these prismatic intrayarn pores are very small, since they are controlled by the inter-fibre spacing. In contrast, the interyarn pores are much larger and exhibit angular shape. Hence, these pores tend to affect significantly the initiation of matrix cracks.

In order to obtain a three-dimensional representation of the complex pore geometry, the distribution of the porosity was studied on the face (width direction), the longitudinal edge (thickness direction) and the transverse edge (cross-section) of the specimens. The histograms of the distribution of pores by surface area and by count are shown for two-dimensional woven composites. The results for all three composites are summarized in Table I and discussed further for each type of composite. The data are divided according to the pore size and histograms of per cent of total count and surface area in each division are plotted. Detailed discussions for each type of composite are given below.

3. Results

3.1. Two-dimensional woven composites

The image analysis software used for this study is able to calculate for each object, i.e. pore, parameters such as location, surface area, dimensions of the major axis of the best fitting ellipse and angle between the major axis and the plane of the fabric layers. The average value and standard deviation for each parameter were calculated based upon a large number of data to achieve a statistical value.

Fig. 2a, b shows micrographs of typical surface areas along the longitudinal edge and face, respectively, of a specimen. The distributions of pores are summarized in Fig. 3a, b. In Fig. 3, the ordinate and abscissa indicate the per cent of total (count, surface area) and the pore surface area ranges, respectively.

Fig. 3a shows data acquired on the longitudinal edge of a composite. In this case, there is a population of large pores, situated at the yarn crossover regions, in the pore size range 0.05–0.5 mm^2 with a peak for the class at the 0.1–0.2 mm^2 range. Another population can be found in the range 0.01–0.05 mm^2 and corresponds to the voids in between two neighbouring layers. The last population, ranging from 0.0001 to 0.01 mm^2, corresponds to residual porosity inside the yarns. The measurement, for more than 1000 pores, of the angle between the major axis of the best fitting ellipse and the plane of the layers gives a value of 2°. Thus, it is concluded that most of the pores are orientated in the plane of the layers.

Fig. 3b depicts the data acquired on the face of a two-dimensional woven composite. Here, the voids exhibit nearly a square shape because of the plain weave fabric structure. The ratio of the lengths of the major axis and the minor axis of the best fitting ellipse is 1.5 and the standard deviation is 0.25. The histogram of the distribution of the voids by count and by surface area shows clearly a bimodal distribution. The first population, with surface areas ranging from 0.05 to 0.14 mm^2, corresponds to the voids in between the yarns; the second one, with surface areas ranging from 0.0001 to 0.01 mm^2, corresponds to the voids inside the yarns.

TABLE I Distribution of pore surface area for the three preform architectures

	Interyarn (mm^2)			Intrayarn (mm^2)		
	Longitudinal edge	Face	Transverse edge	Longitudinal edge	Face	Transverse edge
Two-dimensional woven	0.010 ~ 0.500	0.050 ~ 0.140	0.010 ~ 0.500	0.000 ~ 0.010	0.000 ~ 0.010	0.000 ~ 0.010
Three-dimensional two step braided	0.001 ~ 0.005	0.001 ~ 0.005	0.005 ~ 0.025	0.000 ~ 0.001	0.000 ~ 0.001	0.000 ~ 0.005
Three-dimensional four step braided	0.500 ~ 1.000	0.500 ~ 1.000	0.050 ~ 1.000	0.000 ~ 0.050	0.000 ~ 0.050	0.000 ~ 0.010

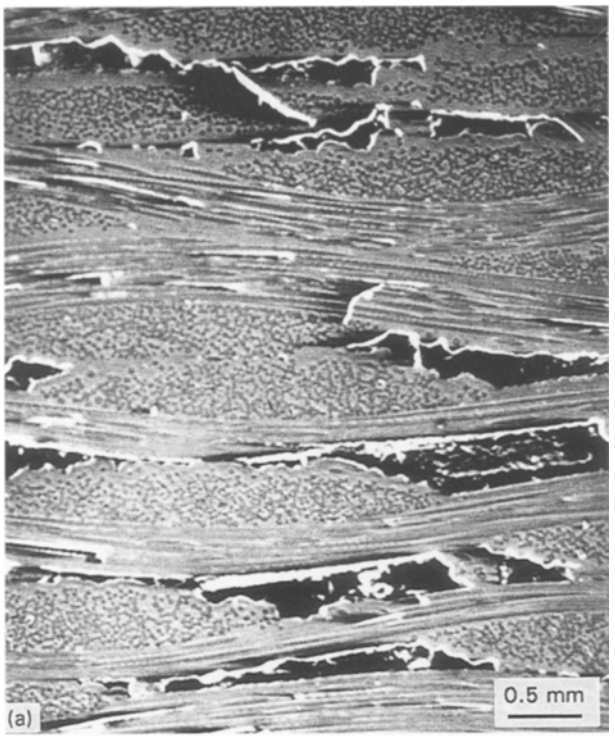

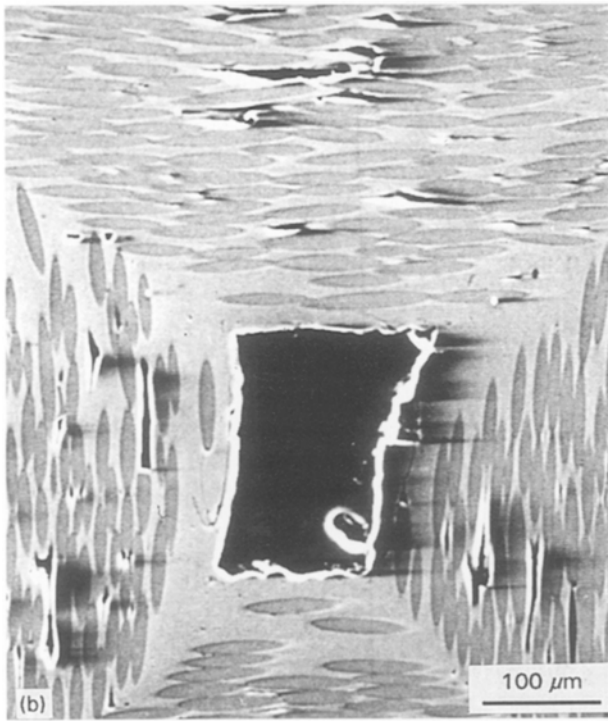

Figure 2 Typical pore geometries observed on surfaces along (a) the longitudinal edge, and (b) the face of the two-dimensional woven SiC–SiC composite.

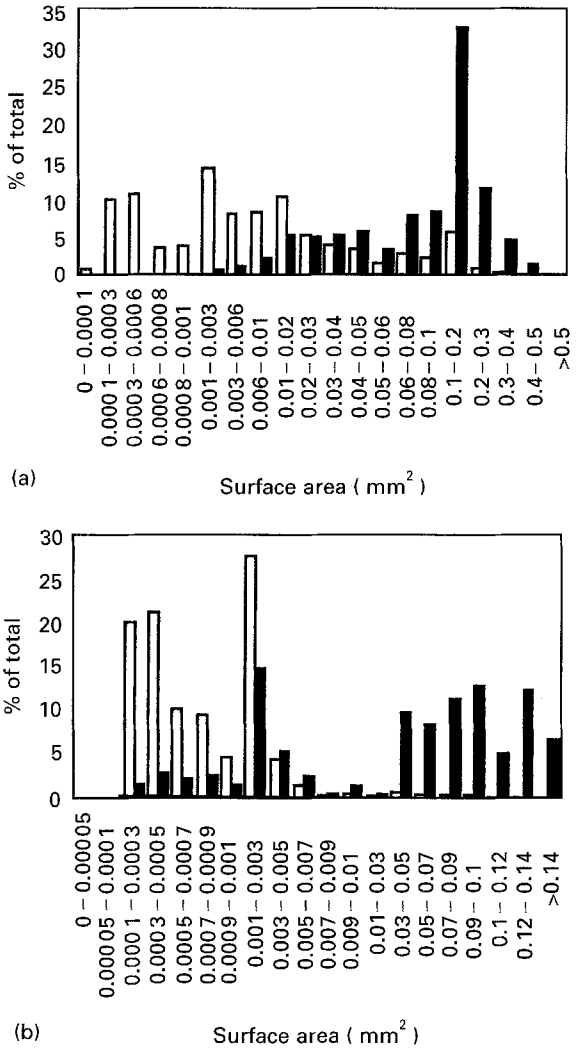

Figure 3 Histograms of pore size distributions on surfaces along (a) the longitudinal edge, and (b) the face of the two-dimensional woven SiC–SiC composites: (□) count in the range, (■) surface area in the range.

3.2. Three-dimensional two step braided composites

The fibre architecture of the three-dimensional two step braided specimen is close to that of the unidirectional composite; 80% of the yarns are aligned along the longitudinal direction and intertwined with the braider yarns. The density of this composite is higher than those of the other two composites. The amount and the size of the pores are smaller, and the pores do not exhibit sharp angles. The histograms for the three-dimensional materials are not shown here, but the results are summarized in Table I.

Analysis of the porosity distribution on the longitudinal edge and on the face of the specimens suggests that the largest pores are located at the crossover regions between axial yarns and braiders. The surface areas lie between 0.001 and 0.005 mm^2 for most of these pores. The surface areas of the intrayarn pores range between 0 and 0.001 mm^2. The pores located on the transverse edge of the specimens are mainly intrayarn pores, with surface areas ranging from 0 to 0.005 m^2. Some pores of larger dimensions, in the range 0.005–0.025 mm^2, can be observed between the yarns.

3.3. Three-dimensional four step braided composites

The shape of the pores for this preform architecture is similar to that of the two-dimensional woven composite. However, because each yarn contains 2000 fibres, the interyarn pores located at the yarn crossover regions are larger.

From the analysis of porosity distribution along the longitudinal edge and the face of the specimens, two populations of pores can be identified. The surface areas of the intrayarn pores are in the range 0–0.05 mm^2. But the surface areas of the interyarn pores are larger, ranging from 0.5 to 1 mm^2. Since the yarns are bigger than those of the two-dimensional woven composite, the open space at the yarn cross-over region is also larger. The shape of the interyarn pores is somewhat different from those of the two-dimensional woven composites; they are thinner and longer. The transverse edge of the specimen again exhibits two populations of pores. The surface areas of the interyarn pores range from 0.05 to 0.1 mm^2, while those for the intrayarn pores are from 0 to 0.01 mm^2.

4. Discussion

4.1. Tensile and compressive behaviour

The two-dimensional woven specimens contained 11 fabric layers and were prepared from 200×200 mm^2 plates. The specimens received a thick coating of SiC matrix during the fabrication process, and their surfaces were rough, thus inhibiting good bonding with strain gauges. Since the removal of part of the external layer would not significantly affect the mechanical response of the material, the specimens were machined in a dog-bone shape, and their surfaces were ground to be smoother and parallel to each other up to half the thickness of a layer on each side. The parallel longitudinal surfaces allow the specimens to be tested without end tabs. The width of the specimens was 10 mm in the tab region and 8 mm in the gauge length. The length of the specimens was 120 mm for tension and 70 mm for compression tests. After machining, the thickness of the specimens was close to 3 mm and there were about ten fabric layers. Despite some irregularities of the surfaces, the three-dimensional specimens were not machined. Grinding the surface would remove a part of the external yarns and disrupt the integrity of the fibre architecture. Strain gauges were bonded on both sides of the specimens at 0 and 90° with respect to the longitudinal axis. The tests were carried out on a testing machine equipped with a hydraulically actuated, wedge-loaded grip system. This system was necessary to minimize bending and/or torsion and avoid damage during clamping of the specimen. The crosshead speed was 0.01 mm min^{-1}.

All of the tests were conducted at room temperature. Some of the specimens were polished on the edge, and a replicating technique was used to characterize damage initiation and evolution under loading. Optical and scanning electron microscopy were used to study the replica as well as the fracture characteristics of the composites. More than ten specimens were used for each test.

4.1.1. Tensile behaviour

Typical tensile stress–strain curves are presented in Fig. 4 for the three types of fibre architectures. The tensile properties of the composites as extracted from the stress–strain curves are summarized in Table II. The characteristics of the tensile behaviour are delineated below.

The Young's moduli, E_{11}, calculated from the initial part of the curves range between 230 and 260 GPa for the three composites. The elastic modulus of the SiC matrix (400 GPa) is twice that of the SiC fibres (about 200 GPa); therefore, a change in the fibre architecture has only a slight effect on the initial modulus of the composite.

The stress, σ_y, at the proportional limit or the onset of non-linearity is 60 and 70 MPa for the two-dimensional woven and the three-dimensional four step braided composites, respectively, and 90 MPa for the three-dimensional two step braided composite. This difference can be explained on the basis of the pore morphology. In the case of the three dimensional two step composites, the progressive coating of the fibre induces longitudinal pores extending along the axial fibre direction. In contrast, in the two-dimensional

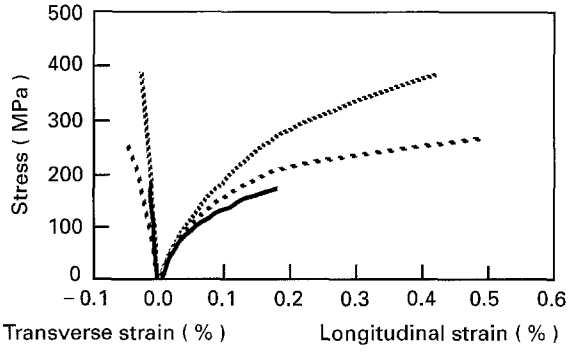

Figure 4 Typical tensile stress–strain curves, giving both longitudinal and transverse strain responses, for the three SiC–SiC composites: (—) two-dimensional woven, (- - - -) two step braided, (...) four step braided.

TABLE II Tensile and compressive properties of the three materials[a]

	Tension					Compression				
	E_{11} (GPa)	υ_{12}	σ_y (MPa)	σ_R (MPa)	ε_R (%)	E_{11} (GPa)	υ_{12}	σ_y (MPa)	σ_R (MPa)	ε_R (%)
Two-dimensional woven	230	0.16	60	180	0.18	230	0.17	700	700	0.28
Three-dimensional two step	260	0.17	90	390	0.42	250	0.15	400	500	0.18
Three-dimensional four step	240	0.22	70	270	0.5	235	0.20	370	390	0.20

[a] E_{11} is the Young's modulus in the loading direction, υ_{12} major Poisson's ratio, σ_y proportional limit, σ_F ultimate strength and ε_R strain to rupture.

woven and the three-dimensional four step braided composites, the void space created by the crossing over of yarns gives rise to more irregular shaped pores. The sharp corners that characterize these types of macropores result in high local stress concentration, which leads to matrix cracking at low levels of applied stress.

Beyond the proportional limit, the three materials exhibit a non-linear behaviour governed by damage mechanisms, such as matrix cracking, delamination between layers, fibre–matrix debonding and fibre breakage. The initiation and evolution of these mechanisms depend on the fibrous structure and are detailed below.

Tensile loading–unloading–reloading clearly showed a progressive decrease in composite stiffness, reflecting an accumulation of damage. Replicas of the edge of the specimens were obtained and examined at various levels of stress. Four phases of damage could be identified for the three materials.

1. phase 1: no apparent damage, some cracking can be detected by acoustic emission, but the behaviour remains linear elastic;
2. phase 2: cracks develop in the matrix rich region between yarn bundles and inside transverse bundles, generally initiating at the pores and running perpendicular to the loading direction;
3. phase 3: multiple cracks appear within the longitudinal yarn perpendicular to the fibre direction;
4. phase 4: fibres start to break, leading to fracture of the specimen.

Phases 1 and 2 are matrix dominated and they are almost similar for the three composites. Phases 3 and 4 are fibre dominated and they are different for the three fibre architectures studied. The evolution of damage during the four phases is represented by the schematic drawings of Fig. 5 for the three composites.

For the two-dimensional woven material, transverse cracks, initiated at the interyarn pores, induce stress concentrations in the longitudinal bundles. These bundles contain only 500 fibres and can not sustain extensive fibre breakage (Fig. 6), causing fracture of the specimen at the strain of 0.2%.

For the three-dimensional two step composites, the interyarn pores are smaller with less sharp corners as compared with two-dimensional woven specimens. As a result, cracks develop first in the matrix rich regions between the bundles until saturation at a crack spacing ranging between 150 and 200 μm (Fig. 7a). Then, microcracks appear inside the bundles, until saturation at a crack spacing close to 30 μm

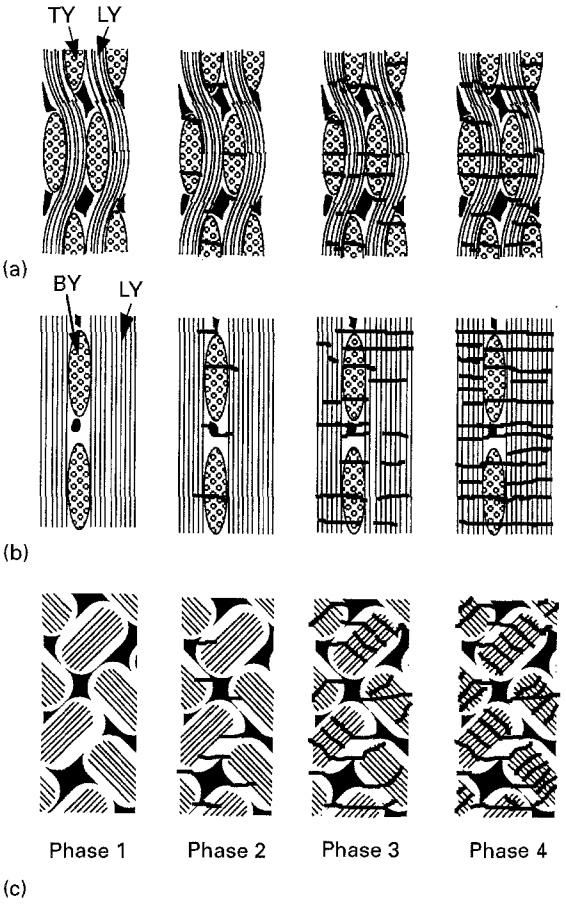

Figure 5 Schematic drawing of the four phases of damage in (a) two-dimensional woven, (b) two step braided, and (c) four step braided composite: TY, transverse yarn; LY, longitudinal yarn; BY, braider of yarn.

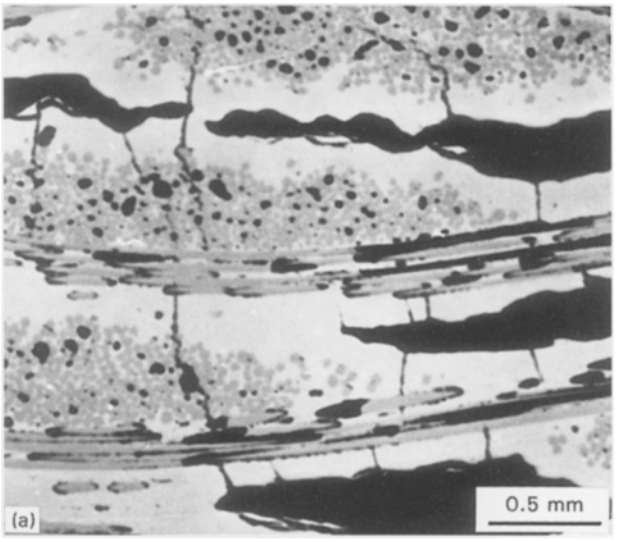

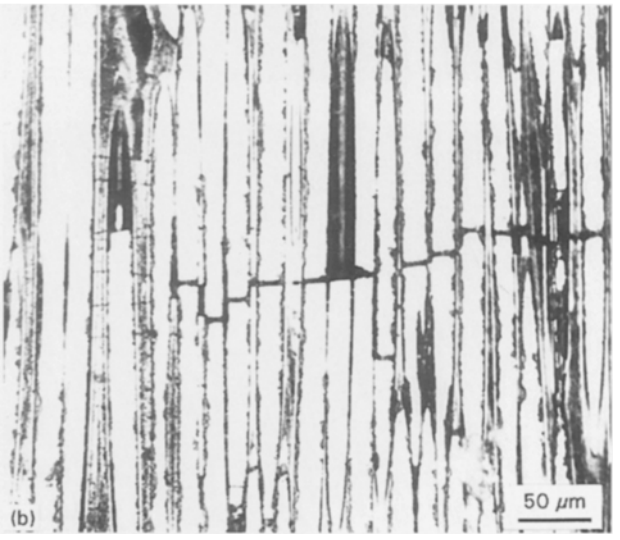

Figure 6 Photomicrographs of the side of a two-dimensional woven specimen showing (a) microcracking in the matrix rich regions initiated by the pores, and (b) microcracks and fibre breakages inside the yarns.

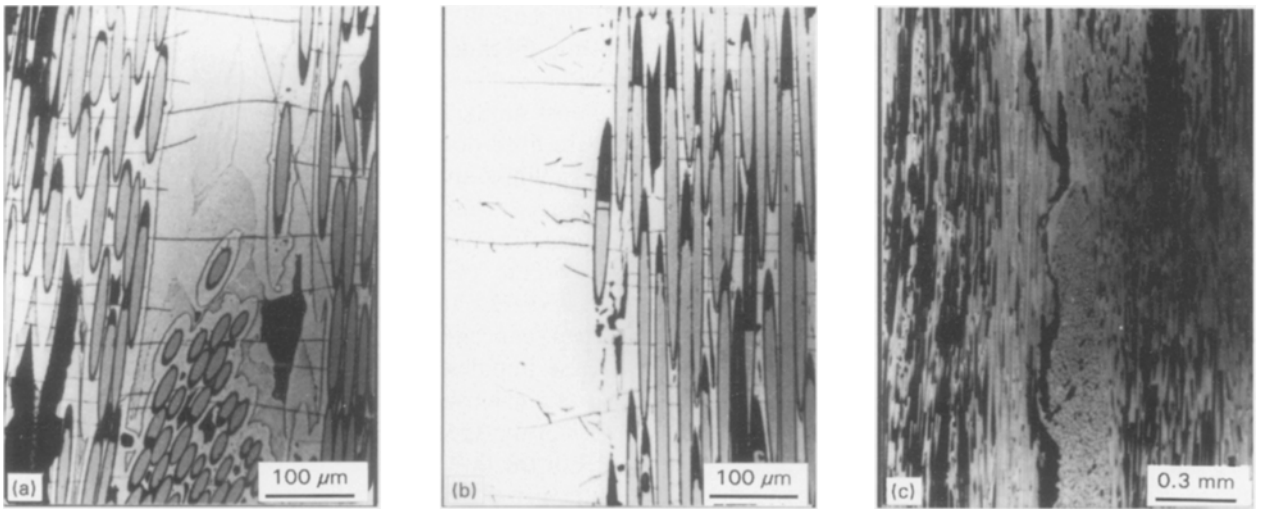

Figure 7 Photomicrographs of the longitudinal edge of a three-dimensional two step braided specimen showing: (a) cracks in the matrix rich regions and in the braider yarns, (b) cracks inside the longitudinal yarns, and (c) delamination between yarns.

(Fig. 7b). The fracture of the specimens occurs at a strain close to 0.4% through fibre breakage as well as separation of the bundles (Fig. 7c).

For the three-dimensional four step braided composite, cracks develop first in the matrix rich regions until saturation at a crack spacing ranging between 150 and 200 μm (Fig. 8a). Then microcracks form inside the bundles perpendicular to the fibre direction. For this fibre architecture, the microcracks are not perpendicular to the loading axis (Fig. 8b). This change of the crack orientation can be detected from the transverse stress–strain curve. The transverse stress–strain curves (Fig. 4) are linear elastic for the two-dimensional woven and the three-dimensinal two step braided composites because the cracks develop perpendicular to the loading direction up to the failure of composites and have little influence on the transverse properties. For the three-dimensional four step composite, the transverse stress–strain curve exhibits a non-linear behaviour because of the orientation of the microcracks.

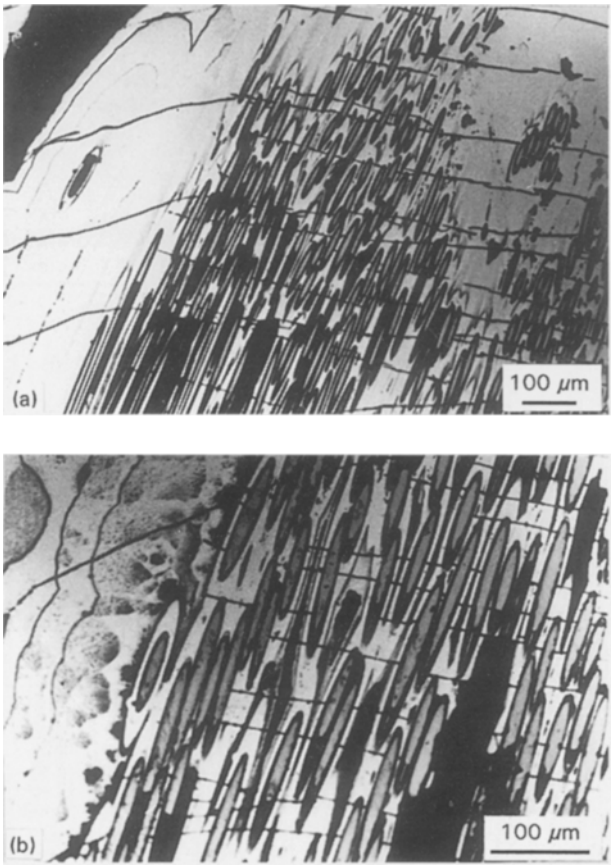

Figure 8 Photomicrographs of the longitudinal edge of a three-dimensional four step braided specimen showing: (a) cracks in the matrix rich regions, and (b) cracks inside the longitudinal yarns, normal to the fibre direction.

4.1.2. Compressive behaviour

The compressive behaviour of the three materials is very different from the tensile behaviour in that it is nearly linear elastic to failure (Fig. 9). The compressive loading closes the cracks, thus no damage was detected until final failure occurred. For the two-step braided material, there was a slight deviation in linearity towards the end of the curve, probably due to the delamination and buckling of the yarns. The two-dimensional woven material exhibited the highest stress and strain to rupture.

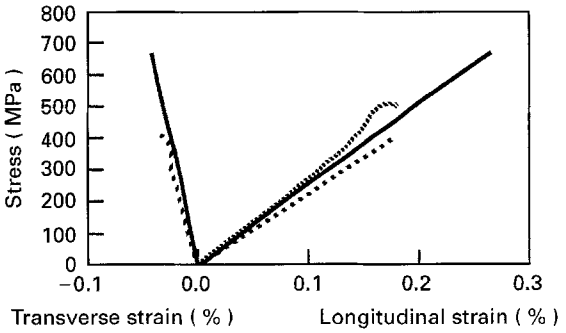

Figure 9 Typical stress–strain curves under compression loading for (—) two-dimensional woven, (- - - -) two step braided and (. . .) four step braided composites.

4.2. Tensile and compressive damage characteristics of two-dimensional woven composites

The purpose of this section is to establish the fundamental damage characteristics of two-dimensional woven composites which would be used for analytical damage modelling [13]. Two aspects of damage characteristic are examined: the degree of isotropic behaviour of the undamaged material, and the coupling between the damages induced in tension and compression.

4.2.1. Quasi-isotropic elastic behaviour

To assess the degree of isotropy in the plane of the fabric layers of the undamaged as well as damaged materials, off-axis tensile tests were performed. The angles between the loading axis and the principal material direction were 10, 20, 30 and 45°. Two to three specimens were tested for each angle. Typical stress–strain curves are presented in Fig. 10, and the key elastic and ultimate properties are summarized in Table III. The stress–strain behaviours of 0, 10 and 20° specimens are quite similar, within the dispersion of the test results. The response of the 30 and 45° specimens is different from that of the others despite a similar linear part. The strain to rupture is similar for all the specimens, 0.184–0.177%. The variation in properties is about 13% for E_{11} (220–193 GPa), about 4% for ultimate strength, σ_R, (180–173 MPa) and 15% for the major Poisson's ratio, υ_{12}, (0.16–0.19).

It is concluded that the linear elastic behaviour of the two-dimensional woven fabric composite can be approximated to be quasi-isotropic in the fabric plane. The damaged material under uniaxial tension behaves as quasi-isotropic until a threshold stress level. This threshold is 120 MPa and corresponds to the end of matrix dominated damage in the composite. Below this stress level, damage is due to matrix cracking in between the yarns. These cracks are perpendicular to the loading direction and their initiation depends upon the amount of matrix between the yarns and the morphology of the interyarn porosity. Above this threshold, microcracking occurs inside the yarns, perpendicular to the fibre direction. The damage mechanisms are then dependent upon fibre orientation.

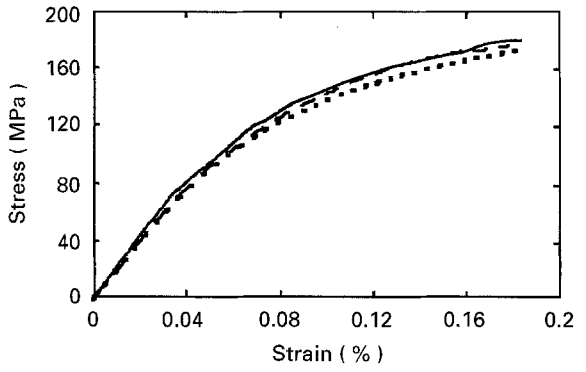

Figure 10 Tensile stress–strain curves for off-axis specimens of two-dimensional woven composite: (—) 0°, (– –) 20°, (- - -) 45°.

TABLE III Off-axis tensile properties of two-dimensional woven composites

Off-axis angle (deg)	E_{11} (GPa)	υ_{12}	σ_R (MPa)	ε_R (%)
0	220	0.16	180	0.183
10	205	0.16	184	0.173
20	200	0.17	177	0.177
30	198	0.18	170	0.184
45	193	0.19	173	0.184

4.2.2. Interdependence of the damage modes

The damage behaviour of SiC–SiC composites under tensile loading can be related to damage mechanisms, such as matrix cracking, fibre–matrix debonding and fibre breakage. On the other hand, under compressive loading, the material exhibits a linear elastic behaviour with no apparent damage. In order to ascertain the coupling between tensile damage and compressive behaviour, compressive tests were performed after a tensile preload on the two-dimensional woven composite. The specimens were preloaded up to 130, 160 and 170 MPa under tension; these values correspond to 70, 85 and 95% of the ultimate strength, respectively. The stress–strain curves corresponding to 160 and 170 MPa preload are presented in Fig. 11, and the results are also summarized in Table IV.

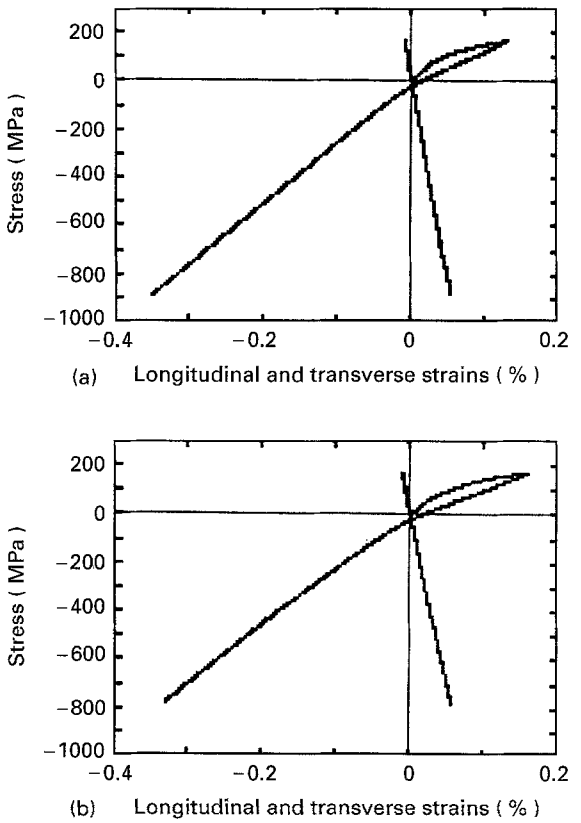

Figure 11 Compressive behaviour after tensile preload to (a) 85% and (b) 95% of the strength. The upper right quadrant in (a) and (b) represents the longitudinal strain response during tensile preloading. The lower left quadrant shows the longitudinal strain response for the compressive-after-tensile loading. The other two quadrants give the transverse strain response for the two loading conditions.

TABLE IV Properties related to compression test after tensile preload[a]

Test no.	Tension						Compression			
	E_0 (GPa)	υ_0	E_{unl} (GPa)	υ_{unl}	σ_{max} (MPa)	ε_{max} (%)	E_0 (GPa)	υ_0	σ_R (MPa)	ε_R (%)
1	220	0.15	156	0.10	130	0.90	220	0.15	− 720	− 0.33
2	240	0.15	136	0.08	160	0.13	240	0.15	− 890	− 0.36
3	230	0.16	115	0.07	170	0.16	230	0.16	− 780	− 0.33

[a] Subscripts "0" and "unl" refer to the initial and unloaded conditions, respectively ; σ_{max} and ε_{max} refer to the maximum stress and strain under tensile loading; σ_R and ε_R refer to the strength and failure strain, respectively, under compressive loading.

When a compressive load is applied, the cracks initiated under tensile loading close completely and do not affect the integrity of the material. The replicas taken under tensile loading clearly showed the presence of the cracks; however, when the specimen was unloaded, no cracks could be detected. Residual deformations after tensile loading can be related to fragments of matrix removed from their initial position. The initial modulus under compression is then reached when the longitudinal strain becomes negative. The essential conclusion from this experiment is that there are no couplings between tension and compression damages for the two-dimensional woven composite when the specimen is loaded in the principal material directions.

4.3. Flexural behaviour of two-dimensional woven composites

The flexural behaviour of two-dimensional woven composites was examined using a four point bend test with a crosshead speed of 0.005 mm min^{-1}. Ten specimens were tested. The specimens had the dimension of $3 \times 4 \times 60$ mm, and the lengths of the inner and outer spans were 25 and 50 mm, respectively. The ratio of the length to the thickness of the specimen, as well as the span length were so chosen as to minimize the shear stresses and to achieve rupture under tension. The load was introduced perpendicular to the layers of the fabric. The strains were measured on both the tension and compression sides of the specimen using strain gauges. The midspan deflection of the beam was also measured on some of the specimens.

A typical load–deflection curve of a two-dimensional woven composite under four-point bending is presented in Fig. 12. Damage mechanisms were characterized through the use of a replicating technique. On the compression side of the beam, no damage could be observed from the replicas. On the tension side, microcracks initiated at the free surface and developed through the thickness of the specimen. The number of cracks versus load on the tension side, within a 10 mm gauge length between the inner spans, is plotted in Fig. 13 for two specimens.

The first cracks can be detected at a loading level close to 120 N, which corresponds to the onset of non-linearity on the load–deflection curves. Then, multiplication of cracks occurs as the load increases. The evolution of microcracking is nearly linear with

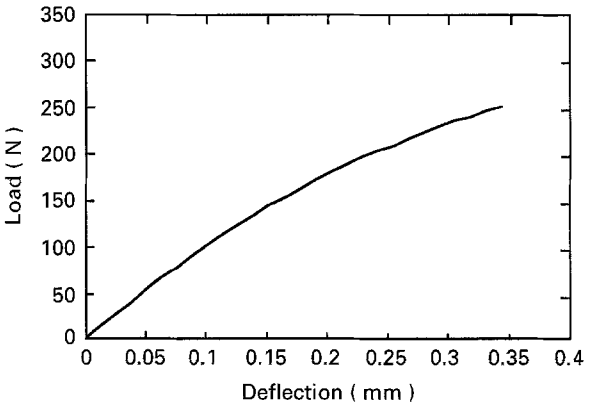

Figure 12 Typical load–displacement curve for two-dimensional woven SiC–SiC specimen under flexure loading.

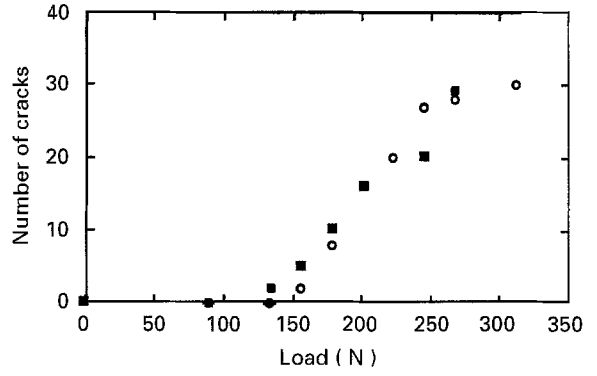

Figure 13 The number of cracks obtained within a 10 mm gauge length between the inner spans of the two-dimensional woven flexure specimen as a function of the applied load: (○) specimen A, (■) specimen B.

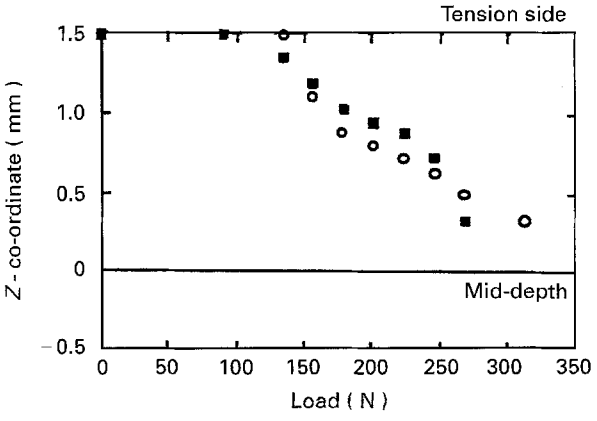

Figure 14 The depth of propagation of microcracks from the tension side through the thickness of the two-dimensional woven flexure specimen as a function of applied load: (○) specimen A, (■) specimen B.

load until saturation at around 270 N. The cracks are almost regularly spaced unless a pore gives rise to more cracks because of stress concentrations. The propagation of a macrocrack through the thickness of the beam leads to the failure of the specimen. The microcracks do not reach the mid-depth of the specimen until just before rupture. Fig. 14 shows the depth to which microcracks have grown as a function of the applied load.

5. Conclusions

The experimental studies of damage mechanisms and evolution in two- and three-dimensional SiC–SiC fabric composites have led to the following conclusions.

1. Although the fibre, the matrix and the infiltration conditions are identical for the three composites, their residual pore morphology and mechanical behaviour are significantly different due to their distinct fibre architectures.

2. The morphological study identifies two main populations of pores: (i) intrayarn pore: the shape of intrayarn pores depends mainly on the degree of densification of the preform, their shape and distribution are similar for the three materials; (ii) interyarn pores: the size and shape of these pores depend on the fibre architecture and can be related to the dimension and waviness of the yarns. For two-dimensional woven composites, the residual pores exhibit sharp corners because the yarn curvature at the crossover region is large. For four step braided composites, the less sharp curvature of the yarns gives rise to more rounded pores. For three-dimensional two step braided composites, the paths of matrix vapour infiltration are straight, and the size of the pores is significantly reduced. Thus, a reduction of yarn waviness provides a less tortuous path of matrix infiltration and lowers porosity.

3. All three types of composites exhibit non-linear behaviour under tensile loading. The damage development is described through different phases. The damage is first matrix dominated, and it is very similar for the three materials. Then, damage becomes fibre dominated and it differs significantly, depending upon the fibre structure. The strain to rupture increases when the number of fibres in the bundles increases and the weaviness is larger. Under compression loading, all three materials are linear elastic up to failure.

4. Off-axis tensile tests show that elastic property variation with angle is less than 15%. Therefore, the in-plane elastic behaviour of two-dimensional woven fabric composites can be approximated to be quasi-isotropic. Furthermore, damage induced by a tensile preload up to 95% of the ultimate strength has no influence on the compressive behaviour of the two-dimensional woven composites. Thus, there is no coupling of damage mechanisms between tension and compression loading along the principal material directions.

Acknowledgements

The authors wish to acknowledge the support of NASA-Lewis Research Center (John Gyekenyesi, Program Manager) and thank Mark Headinger of E. I. Du Pont de Nemours & Co., Inc., for providing the materials and many helpful discussions.

References

1. T. I. MAH, M. G. MENDIRATTA, A. P. KATZ and K. S. MAZDIYASNI, *Amer. Ceram. Soc. Bull.* **66** (1987) 104.
2. A. J. CAPUTO, D. P. STINTON, R. A. LOWDEN and T. M. BESMAN, *ibid.* **66** (1987) 368.
3. N. H. TAI and T. W. CHOU, *J. Amer. Ceram. Soc.* **72** (1989) 414.
4. R. NASLAIN and F. LANGLAIS, *High Temp. Sci.* **27** (2) (1988–1989) 221.
5. M. H. HEADINGER, R. N. KLACKA, S. L. BORS and W. R. MOSCHELLE, in the 17th Annual Conference on Composites and Advanced Ceramics, January 1993, Cocoa Beach, FL.
6. T. W. CHOU, "Microstructural Design of Fiber Composites" (Cambridge University Press, 1992).
7. S. W. WANG and A. PARVIZI-MAJIDI, *J. Mater. Sci.* **27** (1992) 5483.
8. P. G. KARANDIKAR and T. W. CHOU, *Compos. Sci. Technol.* **46** (1993) 253.
9. W. S. KUO and T. W. CHOU, *J. Amer. Ceram. Soc.* submitted.
10. W. S. KUO, W. Y. CHEN, A. PARVIZI-MAJIDI and T. W. CHOU, in Proceedings of the International Gas Turbine and Aeroengine Congress and Exposition: Mechanics of Ceramic Matrix Composites, Paper no. 91-GT-105 (1991).
11. P. PLUVINAGE and J. M. QUENISSET, *J. Compos. Mater.* **27** (1993) 152.
12. F. ABBE, I. CHERMANT, M. COSTER, M. GOMINA and J. L. CHERMANT, *Compos. Sci. Technol.* **37** (1990) 109.
13. H. Z. SHAN, P. PLUVINAGE, A. PARVIZI-MAJIDI and T. W. CHOU, *ASME J. Engng Mater. Technol.* submitted.

Received 4 February 1994
and accepted 22 June 1995